Applied Energy 279 (2020) 115726

Contents lists available at ScienceDirect

Applied Energy

journal homepage: www.elsevier.com/locate/apenergy

Design, modelling, and testing of a vibration energy harvester using a novel half-wave mechanical rectification

Jia Mi, Qiaofeng Li, Mingyi Liu, Xiaofan Li, Lei Zuo *

Department of Mechanical Engineering, Virginia Tech, Blacksburg 24061, USA

HIGHLIGHTS

- A novel half-wave mechanical rectification for vibration energy harvesting.
- Nonlinear dynamics to understand the proposed system and optimize the parameters.
- The power output of the proposed system can double that of full-wave rectification.
- Bench and treadmill tests to verify the model and evaluate the system performance.
- The specific power of can reach 0.4 W/kg under a 4.8 km/h walking speed.

GRAPHICAL ABSTRACT

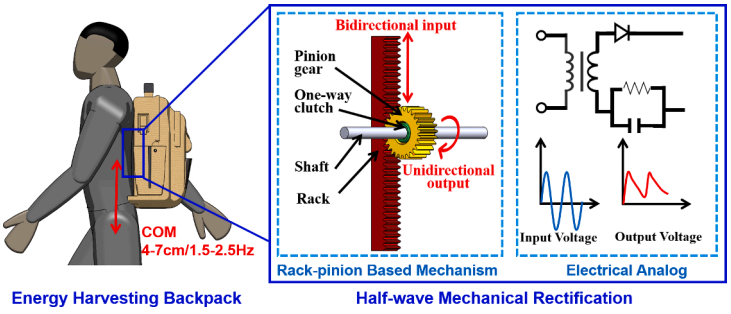

ARTICLE INFO

Keywords:
Biomechanical energy
Energy harvesting
Suspended backpack
Half-wave mechanical rectification
Inertia nonlinearity

ABSTRACT

Portable and wearable electric devices are an important part of our life and the energy supply is critical for their functions. Energy harvesting from human motion is a promising solution to provide the energy supply. This paper presents the design, modeling and testing of a vibration energy harvester using a novel half-wave mechanical rectification to enhance the performance of suspended energy harvesting backpack. The proposed half-wave mechanical rectification mechanism uses one set of rack-pinion and a one-way clutch that converts bidirectional vertical oscillation into unidirectional rotation of the generator with nonlinear inertia. As validated by both modelling and bench tests, the proposed half-wave mechanical rectification-based energy harvesting system can obtain about twofold average output power as the previous full-wave mechanical rectification system in the desired dominant excitation frequency and also maintains larger output power in the target frequency range. The influences of external resistance, human walking speed, and payload mass are also studied to comprehensively characterize the performance and robustness of the proposed design. Treadmill tests on different human subjects demonstrate an average power range of 3.3–5.1 W under a walking speed of 4.8 km/h (3 mph) with a 13.6 kg (30 lbs.) payload. Experimental results indicate that the proposed suspended energy harvesting backpack could continuously generate an amount of electricity suitable for powering portable and wearable electronic devices, which can be applied to the military, field workers, outdoor enthusiasts and disaster relief scenarios.

* Corresponding author.
E-mail address: leizuo@vt.edu (L. Zuo).

https://doi.org/10.1016/j.apenergy.2020.115726
Received 3 May 2020; Received in revised form 22 July 2020; Accepted 18 August 2020
Available online 18 September 2020

Nomenclature

m	payload mass (kg)
m_e	equivalent inerter from generator (kg)
k	spring stiffness (N/m)
R_{ex}	external resistance (Ω)
c_m	mechanical damping (Ns/m)
n	gear ratio
r	radius of pinion gear (m)
R_{in}	internal resistance in generator (Ω)
k_e	speed constant of generator (rpm/V)
k_t	torque constant of generator(Nm/A)
J_g	rotational inertia of the generator (kg·m^2)
θ_g	angular displacement of generator (rad/s)
θ_p	angular displacement of pinion shaft (rad/s)
ω_{in}	input frequency (rad/s)
L	inductance (H)
V	voltage (V)

1. Introduction

Human beings are becoming more and more dependent on portable and wearable electronic devices, and many people seem more concerned with the battery run-time of their electronic devices than with their next meal [1]. In our daily life, we have to replace or recharge batteries for electronics frequently or carry a portable power bank around. However, it might be hard to replace or recharge batteries for some embedded electronic devices, such as cardiac pacemakers and hearing aids [2]. In addition, carrying batteries increases a human's burden. This added weight is undesirable in some situations, such as for hikers, soldiers and field workers who often stay in the field for several days and carry many other loads. As reported by the U.S. Department of Defense (DoD), around 9.1 kg (i.e. 20 lbs.) of batteries are carried for a typical dismounted U.S. soldier on a 72-hour mission [3]. Therefore, the development of longer-lasting or completely self-sustaining power systems has become desirable to reduce the total system size and weight while increasing the functional duration [4]. Different approaches have been investigated to harvest energy from the ambient environment and power portable and wearable electronic devices. The energy sources that exist in the ambient environment include solar energy, thermal energy, and mechanical/kinetic energy [5]. Among them, mechanical/kinetic energy has the largest power density which can reduce the energy harvester size [6]. Therefore, energy harvesting from human motion can achieve a small size and may even reduce a human's burden. Actually, a person's average daily energy expenditure is around 1.1×10^7 J [7], an amount equivalent to approximately 20 kg batteries. That means human motion is an ambulatory and reliable energy source to power electronic devices, and researchers have begun to investigate energy harvesting from human motion, as shown in Fig. 1.

Several studies have been performed to investigate the biomechanical energy harvesting available using active materials or structures. A self-powered triboelectric auditory system was investigated and experimental results showed ultrahigh sensitivity (110 mV/dB) with broadband response which almost covers the frequency range of the human voice (100–5000 Hz) [8]. A muscle-movement-driven nanogenerator was demonstrated and four single wire generators produced an output voltage of up to ~0.1–0.2 V [9]. Study on piezoelectric energy harvesting and storage from motions of the heart, lung, and diaphragm revealed a maximum electrical output power of 0.5 V/43 nA [10]. A two-stage force amplification mechanism was investigated on a novel heel-shaped piezoelectric energy harvester and achieved 24 mW (average)/66 mW (peak) output power [11]. To harvest energy from the swing motion of leg, a magnetic-spring based energy harvester was

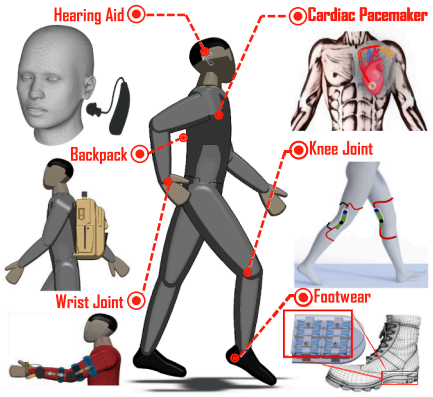

Fig. 1. Biomechanical energy harvesting technologies and applications.

investigated and achieved a maximum average output power of 10.7 mW [4]. A wearable self-powered wireless sensing system was developed with frequency up-conversion through magnetic plucking and experimentally achieved an output power range of 1.9–4.5 mW [12]. Yuan and Zhu [13] developed a self-powered wearable multisensory bracelet incorporating a flexible thermoelectric generator and achieved power performance with power density of 3.5 μW/cm^2. However, the energy harvesting at the milliwatt level using active materials or structures has only limited applications to low-power electronics and self-powered wireless sensors. Therefore, large-scale (>1 W) biomechanical energy harvesting is more desirable to power portable electrical devices in some specific applications, such as the military, field workers, outdoor enthusiasts and disaster relief scenarios.

To harvest large-scale biomechanical energy, several studies have been performed to investigate the energy harvesting from human joints and center of mass (COM) motions. As investigated in reference [14], for a device that uses center of mass motion, the maximum amount of harvestable energy is approximately 1 W per kilogram of device weight; for a joint-mounted device based on generative braking, the joints generating the most power are the knees (34 W) and the ankles (20 W). A knee energy harvester using a gear train and one-way clutch was developed which selectively engages power generation at the end of the swing phase to assist deceleration of the joint and an average power of 5 W experimentally obtained [15]. To harvest energy from center of mass motion, a suspended-load energy harvesting backpack was proposed, which uses a rack-pinion to convert the vertical oscillation into rotational motion of a miniature power generator [16]. The experiments demonstrated up to 7.4 W average power at a 20–38 kg backpack load and little extra metabolic energy was required during electricity generation. The U.S. Army Communications-Electronics Research, Development and Engineering Center (CERDEC) developed and tested a harvesting assault pack using a double frame load suspension system [17], and an average power of about 2 W was obtained under 4.8 km/h (i.e. 3 mph) walking with a 15.9 kg (i.e. 35 lbs.) backpack load. Kuo claimed useful amount of electrical power could be generated from suspended-load energy harvesting backpacks while costing less metabolic energy than would be expected [1].

As for the energy harvesting from center of mass motions, the primary frequency of human center of mass motion in walking is about 2 Hz [18,19]. However, this frequency varies from 1.5 Hz to 2.5 Hz depending on walking speed, road condition, gender, height and weight et al. Beside the excitation frequency, varying payload mass will also affect the natural frequency and the performance, similar to that in a suspension energy harvesting system [20,21]. For example, the payload of a U.S. soldier's backpack varies from 6.8 kg to 61.2 kg (15–135 lbs.) [3,17], which means the natural frequency can change by three times. For the design of a suspended backpack, the payload mass and desired dominant working frequency are typically preselected first, and the

spring stiffness and electrical damping (i.e. external resistance) are then determined so that the natural frequency of the system matches to excitation frequency. Researchers found the energy harvesting performance will suffer as the excitation frequency deviates from the resonance frequency [22,23] and it is difficult to achieve good performance through linear systems since the real excitation generated by human motion exhibits a degree of randomness and time variance [24]. In addition, the human center of mass motion in walking is up-and-down linear motion. However, a comparative study between a linear and a rotary vibration energy harvester (VEH) found that the rotary vibration energy harvester could achieve larger energy density [25]. Also, the bidirectional oscillating motion will produce an irregular AC voltage. In order to charge batteries or power portable and wearable electronics, the voltage needs to be commutated with an electrical rectifier, in which the forward voltage of diodes unavoidably reduces the circuit's efficiency [26]. Therefore, the mechanical energy from the surrounding environment often needs to be appropriately processed in the mechanical domain and then be converted to electrical energy by common electromechanical energy transducers [27]. To address the aforementioned problems, a mechanical motion rectification (MMR) is applied on backpacks to convert bidirectional linear motion into unidirectional rotation while also achieving broadband via nonlinear inertia [28,29]. The MMR mechanism consists of a rack-pinion set coupled with two one-way clutches to convert the irregular linear oscillation into a regular unidirectional rotation, which is in analogy a full-wave AC/DC electrical rectifier using a center-tapped transformer and two diodes [26]. Due to engagement and disengagement between the shaft and one-way clutches, the inertia of the system alternatively becomes variable, resulting in piecewise linear inertia. With the inertia nonlinearity, MMR-based systems can achieve broadband energy harvesting performance. Both bench tests and treadmill tests confirmed the MMR-based backpack generates energy in broader bandwidth than the linear counterparts [3].

In order to achieve good performance under bidirectional oscillating and broadband excitation, appropriate processing and modulations in the mechanical domain [27] should be investigated for an energy harvesting backpack. Based on the authors' observations and our recent research [30,31], this paper proposes a suspended energy harvesting backpack using a novel half-wave mechanical rectification to convert bidirectional motion into unidirectional rotation and enhance performance under broadband excitation in real walking conditions through nonlinear inertia. On the contrary to previous approaches in full-wave mechanical rectification mechanism which harvest energy in both upward and downward strokes, the proposed half-wave mechanical rectification mechanism only converts the relative vibration in one direction while staying idle in another direction. The dynamics of the proposed system is more complicated when compared with linear systems because of the nonlinear characteristics though engagement and disengagement of the half-wave mechanical rectification, and the system parameter optimization and performance are not understood yet. Therefore, the contributions and novelties of this paper are (1) to introduce a novel design of half-wave mechanical rectification for vibration energy harvesting , (2) to investigate the system dynamics, nonlinear characteristics and the optimal parameters, (3) to experimentally valid the design and assess the pros and cons of the energy harvesting backpack with half-wave mechanical rectification, and (4) to comprehensively characterize the performance and robustness of the proposed design via investigating the influences of external resistance, human walking speed, and payload mass.

Through modelling and simulation, we will find that the proposed energy harvesting backpack using half-wave mechanical rectification can obtain about twofold average output power as the previous full-wave mechanical rectification and traditional non-rectification designs, while maintaining larger output power in the desired frequency range. A backpack prototype is created with a weight of the energy conversion mechanism about 550 g. Bench test results indicate the proposed half-wave mechanical rectification-based energy harvesting backpack can harvest 6.7 W (peak)/2.1 W (average) under 2 Hz/6 mm base-excitation with a 31.8 kg payload, which is a significant improvement compared with 1.9 W (peak)/0.9 W (average) for the counterpart full-wave mechanical rectification based system. At the same time, the bench test results validate the proposed half-wave mechanical rectification design can maintain larger output power in the broad bandwidth frequency range of interest. Finally, treadmill tests on different human subjects demonstrate an average power range of 3.3–5.1 W under a walking speed of 4.8 km/h (3 mph) with a 13.6 kg (30 lbs.) payload.

The rest of this paper is organized as follows. Section 2 introduces the detailed design and working principle of the proposed rack-pinion-based half-wave mechanical rectification harvester. Section 3 introduces the systematic modeling for the proposed energy harvesting backpack using half-wave mechanical rectification. Section 4 summarizes the bench and treadmill tests of the proposed energy harvester. Section 5 provides the concluding remarks.

2. Design principle

Fig. 2 shows the design principle of the proposed rack-pinion based vibration harvester using half-wave mechanical rectification. The harvester consists of a rack-pinion set, a one-way clutch integrated with a shaft, three roller sets, and an electromagnetic (EM) generator with a planetary gearhead. The one-way clutch is between the shaft and pinion gear, which will only transmit torque in one direction. The shaft is supported by bearings and connected with the planetary gearhead by a coupler. Two pairs of side rollers and one pair of back rollers are used to guide the rack's vertical movement while constraining movement from other degrees of freedom. A slice of polytetrafluoroethylene (PTFE) is positioned between the rack and bottom plate to reduce contact friction. A flywheel can be connected to the electric generator rotor to adjust the inertia, as investigated in [32,33].

The bottom plate can be mounted on a fixed part and the connector can be connected to a moving part. The relative movement between the fixed part and moving part can drive the rack moving bidirectionally. Since the one-way clutch will only transmit torque in one direction, the one-way clutch will be disengaged, resulting in no driving torque on the shaft when the rack moves down. When the rack moves up, the one-way clutch will be engaged and the shaft will be driven by the pinion gear. The system will only be engaged in one stroke, therefore, as the rack moves up and down, the shaft will only rotate unidirectionally. The design principle of full-wave mechanical rectification can be found in [28,29], where it can be seen that there are two sets of rack-pinions and two one-way clutches. The full-wave mechanical rectification can also convert bidirectional oscillation into unidirectional motion. The difference is the full-wave mechanical rectification system can be engaged in both up and down strokes while the half-wave system will only be engaged in one stroke. Detailed analysis and comparison can be found in Section 3.

3. Modelling and dynamics

Fig. 3 shows the proposed dynamic modelling of the electromagnetic-generator-based vibration energy harvester using half-wave mechanical rectification. As investigated in [28,29], there are two main forces from the harvester to the whole vibration system at engaged case: damping force F_{EMF} induced by back electromotive current and inertia force $F_{inertia}$ induced by the inertia of rotational parts in generator. The damping force induced by back electromotive current is proportional to the vertical linear velocity of the rack $\frac{dz}{dt}$ and counteracting force induced by the inertia of rotational parts is proportional to the acceleration of the rack $\frac{d^2z}{dt^2}$, as shown in Eq. (1).

$$F_{harvster} = F_{EMF} + F_{inertia} = c_e\frac{dz}{dt} + m_e\frac{d^2z}{dt^2} \quad \text{Engagement} \tag{1}$$

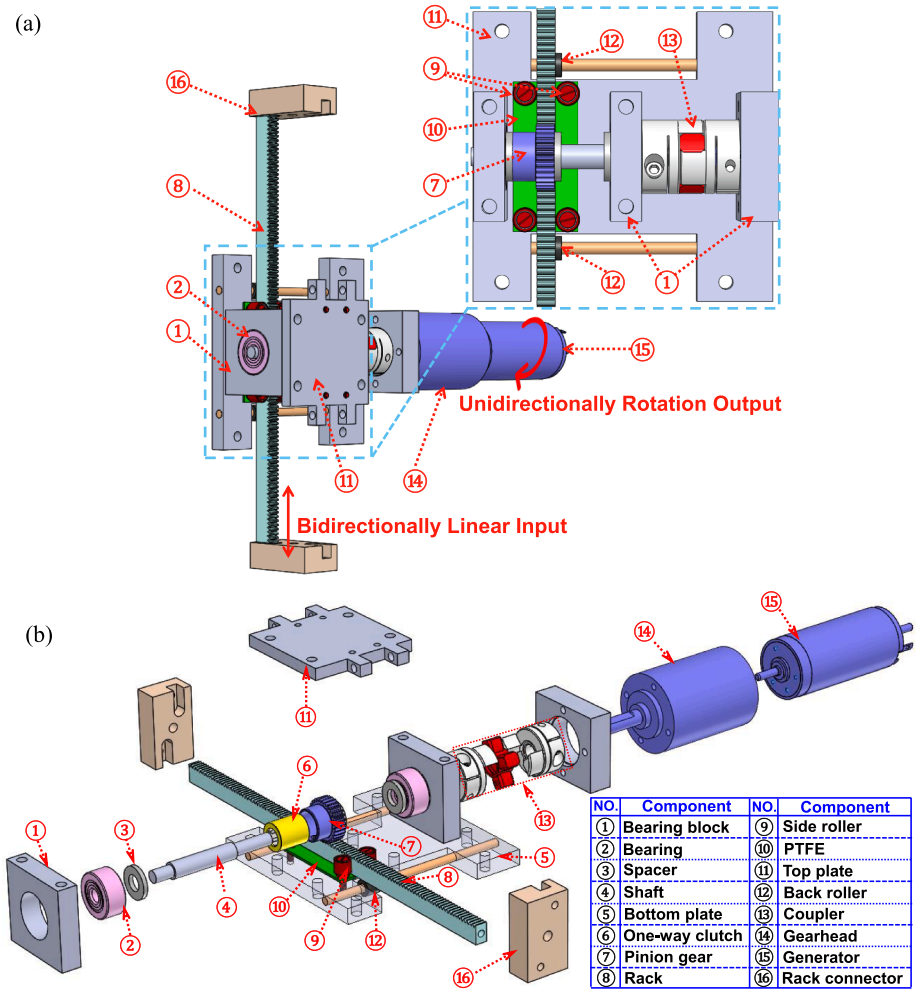

Fig. 2. Design principle of half-wave mechanical rectification-based vibration energy harvester using a rack-pinion mechanism and a one-way clutch: (a) Harvester assembly, (b) Exploded view.

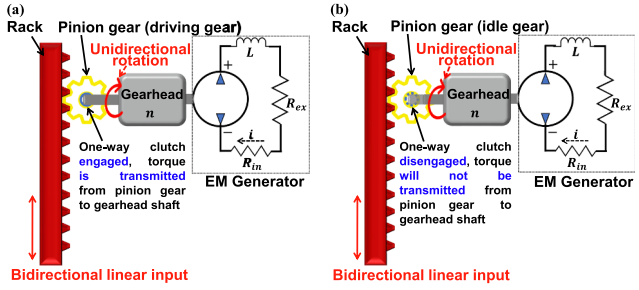

Fig. 3. Dynamic model of the electromagnetic-generator-based vibration energy harvester using half-wave mechanical rectification (a) engaged case (b) disengaged case.

where $c_e = k_t k_e n^2/((R_{ex}+R_{in})r^2)$ is the equivalent electrical damping, $m_e = J_g n^2/r^2$ is the equivalent mass [26], z is the displacement of the rack, k_t is the torque constant of the generator, k_e is the speed constant of the generator, n is the gear ratio in the gearhead, and r is the radius of the pinion gear, J_g is the rotational inertia of the generator, and R_{ex} and R_{in} are the external resistance and internal resistance of the generator, respectively.

As shown in Eq. (1), the gear ratio in gearhead allows positive real impedance (i.e. equivalent mass) to be synthesized mechanically using physical components which may be assumed to have small mass compared to other structures to which they may be attached [34]. It should be noted that, the inertia of the coupler is very small compared with inertia in the generator, so we only consider inertia from the generator if no flywheel is attached.

When the pinion gear is decelerating to an extent that the rotational velocity of the generator shaft becomes larger than that of the pinion gear, i.e., $\frac{d\theta_g}{dt} > \frac{d\theta_p}{dt}$ or $\frac{d\theta_g}{dt} > -\frac{d\theta_p}{dt}$, where $\frac{d\theta_g}{dt}$ is the rotational speed of generator shaft and $\frac{d\theta_p}{dt} = \frac{dz/dt}{r}$ is the rotational speed of pinion gear, respectively, disengagement occurs. As for the disengaged case, the whole system will be decoupled into two separated systems, as shown in Fig. 3(b). In this case, there is no counteracting force from the harvester to the vibration system and the generator will rotate under the two interactional forces.

$$m_e \frac{d^2\theta_g}{dt^2} = -c_e \frac{d\theta_g}{dt} \quad \text{Disengagement} \tag{2}$$

Hence, the rotational speed of the generator shaft will decay as a certain ratio during disengaged case

$$\frac{d\theta_g}{dt} = \frac{d\theta_g^{dn}}{dt} e^{-\frac{t-t_{dn}}{\tau_e}} \tag{3}$$

where $\frac{d\theta_g^{dn}}{dt}$ is the rotational speed of the generator shaft when disengagement happens, t_{dn} is the moment when disengagement happens, and τ_e is the decay ratio where $\tau_e = J_g(R_{ex}+R_{in})/k_t k_e = m_e/c_e$.

The system will be engaged again once the rotational speed of the pinion gear $\frac{d\theta_p}{dt}$ equates the rotational speed of the generator shaft $\frac{d\theta_g}{dt}$. Fig. 4 shows the system modelling of the proposed electromagnetic-based vibration energy harvesting backpack using half-wave mechanical rectification under base-excitation $\mathrm{x} = \mathrm{X}\sin\omega_{\mathrm{in}}\mathrm{t}$, where X is the input amplitude and ω_{in} is the input frequency. As stated earlier, there are engagement cases and disengagement cases in different conditions because of the characteristics of the one-way clutch. During the engagement cases, there are two main forces from the harvester to the whole vibration system and the dynamics of the system is the same as a traditional non-rectification system. During the disengagement period, the generator rotor will be decoupled with the rack-pinion and the whole system will be two independent systems. The payload and spring will be a single vibration system with mechanical damping, and the generator with external resistance will be another independent system. The two decoupled systems will be coupled again when the input speed of the pinion gear is equal to the generator rotor. Therefore, the vibration system is a piece-wise linear system because of the engagement and disengagement of the one-way clutch.

During the engaged case ($\frac{d\theta_g}{dt} = \left|\frac{d\theta_p}{dt}\right|$), the equation of motion can be written as

$$\mathrm{m}\frac{d^2y}{dt^2} + m_e\left(\frac{d^2y}{dt^2} - \frac{d^2x}{dt^2}\right) + (c_e + c_m)\left(\frac{dy}{dt} - \frac{dx}{dt}\right) + k(y - x) = 0 \quad \text{Engagement} \tag{4}$$

where m is the suspended mass,m_e is the equivalent mass, k is the spring stiffness, c_m is the mechanical damping of the system, x, $\frac{dx}{dt}$ and $\frac{d^2x}{dt^2}$ are the displacement, velocity and acceleration of the input, respectively, and y, $\frac{dy}{dt}$ and $\frac{d^2y}{dt^2}$ are the displacement, velocity and acceleration of the suspended mass, respectively.

The relative displacement between the input and suspended mass can be seen as $z = y - x$, and the relative velocity and acceleration can be written as $\frac{dz}{dt} = \frac{dy}{dt} - \frac{dx}{dt}$ and $\frac{d^2z}{dt^2} = \frac{d^2y}{dt^2} - \frac{d^2x}{dt^2}$, respectively. The equation of motion considering relative motion can be written as

$$(\mathrm{m} + m_e)\frac{d^2z}{dt^2} + (c_e + c_m)\frac{dz}{dt} + kz = -m\frac{d^2x}{dt^2} \quad \text{Engagement} \tag{5}$$

During the disengaged case ($\frac{d\theta_g}{dt} > \frac{d\theta_p}{dt}$ or $\frac{d\theta_g}{dt} > -\frac{d\theta_p}{dt}$), the one-way clutch will be idle and the whole system will be decoupled into two sub-systems. The rotation velocity of the generator follows an exponential decay during disengagement because the generator will not be driven by the input shaft while it keeps outputting energy to the resistive load. The equation of motion at the disengaged case can be written as

$$\begin{cases} \mathrm{m}\frac{d^2z}{dt^2} + c_m\frac{dz}{dt} + kz = -m\frac{d^2x}{dt^2}, m_e\frac{d^2\theta_g}{dt^2} = -c_e\frac{d\theta_g}{dt} \\ \frac{d\theta_g}{dt} = \frac{d\theta_g^{dn}}{dt}e^{-\frac{t-t_{dn}}{\tau_e}}, \tau_e = \frac{m_e}{c_e} \end{cases} \text{Disengagement} \tag{6}$$

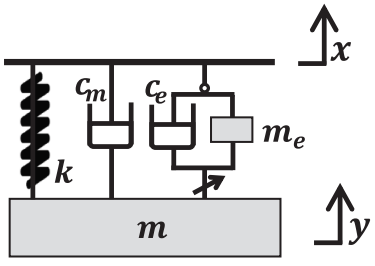

Fig. 4. Modelling of the nonlinear vibration energy harvesting system using one-way clutch.

Because of the piece-wise linear characteristic, it is difficult to find a closed-form solution. The average output electricity can be calculated numerically.

The function of engagement and disengagement of one-way clutch in mechanical domain can be modeled as a diode in electrical domain [28,29]. The threshold of engagement and disengagement of the one-way clutch is determined by velocity in the mechanical domain while the on and off state of diode is determined by current in the electrical domain. In addition, the function of gearhead in the mechanical domain to amplify the rotational speed can also be modelled as the center-tapped transformer in the electrical domain. Therefore, the proposed half-wave mechanical rectification with one one-way clutch can be analogous to a half-wave AC/DC electrical rectifier using one diode while the MMR mechanism with two one-way clutches is in analogy a full-wave AC/DC electrical rectifier using a center-tapped transformer and two diodes. The electromagnetic-based vibration energy harvesting system using one-way clutch can be analogous to electrical circuit with center-tapped transformer and electrical AC/DC filter based on Kirchhoff's current law, and the equivalent terms are shown in Table 1. The equation of motion in engagement case is shown in Eq. (7).

$$\begin{cases} (\mathrm{m} + m_e)\frac{dv}{dt} + (c_e + c_m)v + k\int v = -m\frac{d^2x}{dt^2} & \text{Mechanical domain} \\ (C + C_e)\frac{dV}{dt} + \frac{1}{\mathrm{R} + R_e}V + \frac{1}{L}\int V = i & \text{Electrical domain} \end{cases} \tag{7}$$

The modelling of electromagnetic vibration energy harvesting system using full-wave mechanical rectification is the same as shown in Fig. 4. The difference between full-wave mechanical rectification with two one-way clutches and half-wave mechanical rectification with one one-way clutch is the threshold between engagement and disengagement. Because there are two rack-pinion sets with two one-way clutches in full-wave mechanical rectification mechanism, the system can be engaged in both upward and downward strokes. There is only one set of rack-pinion with one-way clutch in half-wave mechanical rectification mechanism, the system can be engaged in either upward stroke or downward stroke. The threshold of the engagement and disengagement for half-wave mechanical rectification with single one-way clutch can be written as

$$\frac{d\theta_g}{dt} \geq \frac{d\theta_p}{dt} \quad \text{or} \quad \frac{d\theta_g}{dt} \geq -\frac{d\theta_p}{dt} \tag{8}$$

The plus or minus sign depends on the installation direction of the one-way clutch.

The threshold of the engagement and disengagement for full-wave mechanical rectification is different from a half-wave mechanical rectification system because of the two one-way clutches. The threshold for the full-wave mechanical rectification system could be written as

$$\frac{d\theta_g}{dt} \geq \left|\frac{d\theta_p}{dt}\right| \tag{9}$$

Fig. 5 shows the dynamic model of a traditional non-rectification electromagnetic-generator-based vibration system under base-excitation. In traditional non-rectification electromagnetic-generator-based system, there is no one-way clutch and the shaft is rigidly connected with the pinion gear, so the rack will drive the generator directly.

Table 1
Equivalent terms of electrical and mechanical domain (force-current).

Mechanical Domain		Electrical Domain	
m, m_e	Mass	C, C_e	Capacitor
c_e, c_m	Damping	$1/(\mathrm{R} + R_e)$	Resistance
k	Spring	$1/L$	Inductor
v	Velocity	V	Voltage
F	Force	i	Current

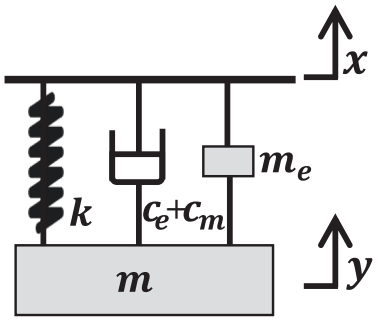

Fig. 5. Modelling of traditional electromagnetic-generator-based vibration energy harvesting system.

The traditional non-rectification system can be seen as a linear vibration system and the equation of motion can be written the same as Eq. (5), and the average output power can be solved by closed-form solution [28]

$$P_{ave}^{non-rectification} = \frac{1}{2} c_e \frac{m^2 \omega_{in}^6 X^2}{\left[k - (\mathrm{m} + m_e)\omega_{in}^2\right]^2 + (c_e + c_m)^2 \omega_{in}^2} \tag{10}$$

The comparison among traditional non-rectification system, full-wave mechanical rectification with two one-way clutches and half-wave mechanical rectification with one one-way clutch can be seen in Table 2.

4. Experiment and evaluation

4.1. Bench tests

To evaluate the performance and characteristic of the proposed system, bench tests were carried out on an Instron machine (model 8801), as shown in Fig. 6. It should be noted that the actual center of mass displacement of human walking is about 4–7 cm [1]. Bench tests were only carried out with low amplitude (6 mm) to analyze the characteristics and treadmill tests with large displacement will be introduced later. As investigated in [3,17], the payload of the backpack varies from 6.8 kg to 61.2 kg (15–135 lbs.), hence, the payload mass was set as 31.8

Table 2
Comparison of three different systems: traditional non-rectification; full-wave rectification; half-wave rectification.

	Traditional non-rectification	Full-wave rectification	Half-wave rectification
System Dynamics	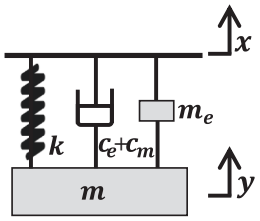	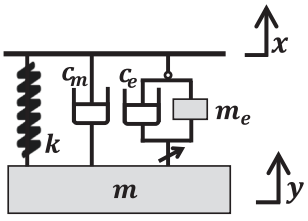	
Equation of Motion	$(\mathrm{m} + m_e)\ddot{z} + (c_e + c_m)\dot{z} + kz = -m\ddot{x}$	Engagement $(\mathrm{m} + m_e)\ddot{z} + (c_e + c_m)\dot{z} + kz = -m\ddot{x}$ Disengagement $\begin{cases} m\ddot{z} + c_m\dot{z} + kz = -m\ddot{x}, \\ \dot{\theta}_g = \dot{\theta}_g^{dn} e^{-\frac{t - t_{dn}}{\tau_e}}, \tau_e = \frac{m_e}{c_e} \end{cases}$ $\dot{\theta}_{in} \geq \left\lvert \dot{\theta}_g \right\rvert$	
Threshold	N/A		$\dot{\theta}_{in} \geq \dot{\theta}_g \text{or} \dot{\theta}_{in} \geq -\dot{\theta}_g$
Mechanism	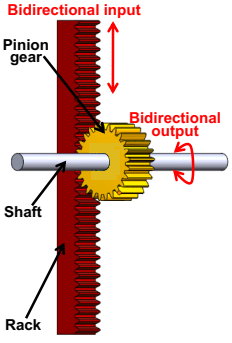	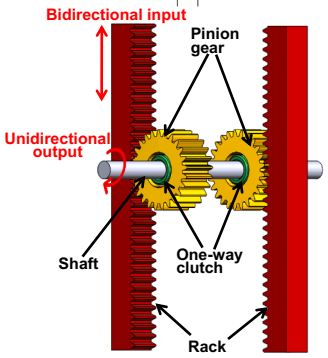	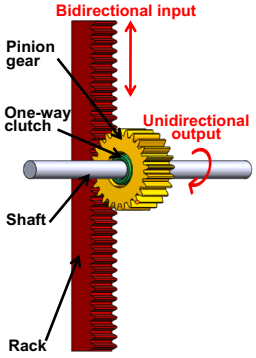
Electrical Analogue	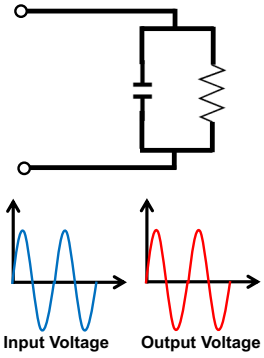	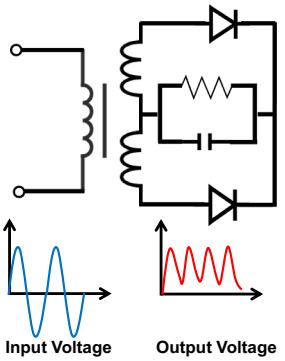	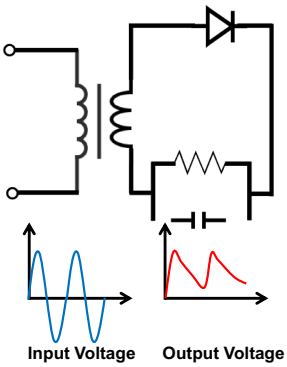

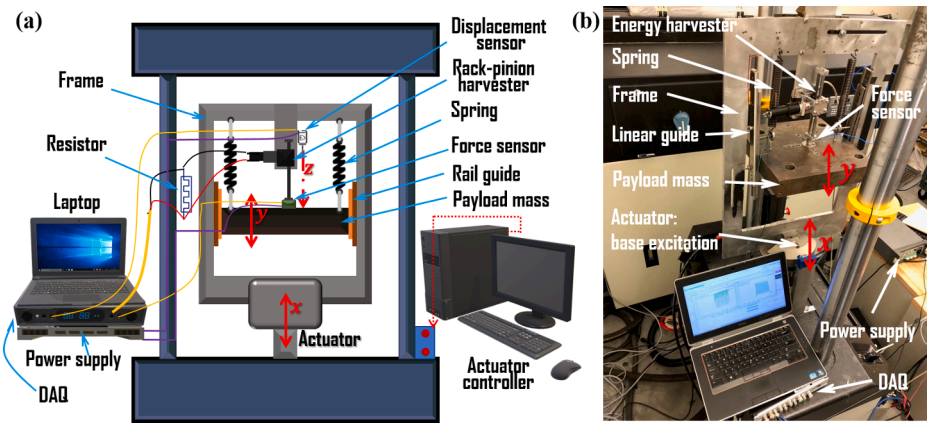

Fig. 6. Bench test (a). Diagram (b). Test set-up.

kg (i.e. 70 lbs.) in bench tests. The electromagnetic-generator used in the harvester is a direct current motor used in the reverse mode. To guide the payload mass and make sure it moves in the vertical direction, a frame with linear rail guides was used and the whole system was clamped to the lower grip of the test machine. The harvester was mounted on the frame, the upper-ends of the springs were connected on the frame and the lower-ends of the springs were connected with the payload mass. A force sensor (PCB 208C03) was connected between the lower end of the rack and payload mass to measure the harvester force impacting to payload mass. A laser displacement sensor (Micro-Epsilon 1302) powered by the power supply measured the relative displacement between the frame and payload mass. To characterize the mechanical damping of this system, a certain input was provided to measure the displacement of the payload mass. Then, a numerical method was adopted to fit the displacement with the experiment results, and it was found the mechanical damping of the system was 85 $\mathrm{Nsm^{-1}}$. The total weight of the harvester is less than 550 g, where the generator (Maxon #118740) with gearhead (Maxon #166163) is about 400 g and the rack-pinion set with frame is about 150 g. As for the DAQ, a USB-6343 Multifunction I/O Device (16 channels) with LabVIEW software was used to collect the data (sampling frequency 100 Hz). Finally, all the data was processed and analyzed via MATLAB.

Since the desired primary frequency is 2 Hz for human walking [18,19], numerical methods were used to determine optimal spring stiffness and electrical damping (i.e. external resistance) for the primary frequency. In the numerical simulation, the governing equations of the two system states are reformulated into explicit discrete state-space representations. Fig. 7 shows the numerical simulation results of average power versus spring stiffness and external resistance under 6 mm/2 Hz base excitation with a 31.8 kg payload mass. From Fig. 7, we can see that the half-wave mechanical rectification system can achieve about 1.8 W average power while only 1.2 W for the counterparts under the same payload mass and excitation conditions (6 mm/2 Hz). In addition, the traditional non-rectification system has the largest optimal spring stiffness (about 8200 N/m), the half-wave mechanical rectification system has the smallest optimal spring stiffness (about 6000 N/m), and the optimal spring stiffness for the full-wave mechanical rectification system is about 6500 N/m. However, since it is hard to get commercialized springs with the exact stiffness needed, a stiffness of 6300 N/m was chosen for both systems. In addition, the optimal electrical damping of the proposed half-wave mechanical rectification system is larger (i.e. smaller external resistance) than full-wave mechanical

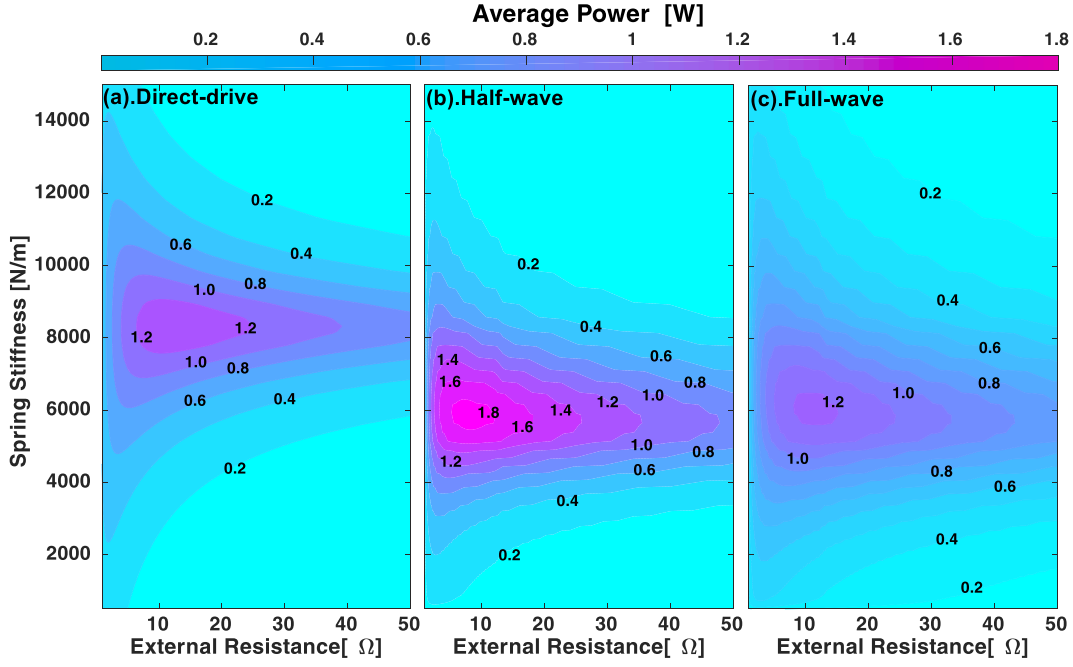

Fig.7. Average power versus spring stiffness and external resistance under 6 mm/2Hz base excitation with a 31.8 kg payload mass.

rectification system and the traditional non-rectification. The system parameters are shown in Table 3.

The bench test results under 2 Hz/6 mm are shown in Figs. 8–10. Each test run 20 cycles and we analyzed the stable period. Fig. 8 shows the numerical and test results of the displacement for both the full-wave mechanical rectification and half-wave mechanical rectification. It shows the bench test results match with the modeling and simulation results with acceptable error. Under the same excitation condition, the half-wave mechanical rectification has larger displacement compared with full-wave-rectification. In addition, the displacement of the proposed half-wave rectification system is asymmetrical in upward and downward strokes while symmetrical for full-wave mechanical rectification system. The reason is the half-wave mechanical rectification design will only have resistive forces from the harvester to the payload in one stroke, while the full-wave mechanical rectification design has resistive force from the harvester in two strokes. Fig. 9 shows the numerical and test results for output power. The average power for the half-wave mechanical rectification system is 2.1 W and 0.9 W for the full-wave mechanical rectification system. It should be noted that, the same harvester was used to maintain the same mechanical damping for both the full-wave mechanical rectification and half-wave mechanical rectification. However, since there are two rack-pinion sets with two one-way clutches in the full-wave mechanical rectification system, one one-way clutch is replaced by an idle bearing for the half-wave mechanical rectification system. That means there are two gear pairs for both the full-wave mechanical rectification and half-wave mechanical rectification systems to maintain the same mechanical damping, while only one one-way clutch will transmit torque in the half-wave mechanical rectification system. In a real application, the half-wave mechanical rectification system only needs one rack-pinion set with one one-way clutch, as shown in Fig. 2.

Fig. 9 shows that the output power results for both the half-wave mechanical rectification system and full-wave mechanical rectification system will drop down near peak point for a while and move up again. The explanation may lie in the imperfect connection between the harvester rack and the payload at the force sensor place. Similar jump phenomenon can also be found in reference [28], in which the same connection methods were used. Such phenomenon did not happen in the treadmill tests (Fig. 9) after we modified the connection between harvester rack and payload.

To investigate the frequency response, sweep sine tests were done to both full-wave mechanical rectification and half-wave mechanical rectification systems, as shown in Fig. 10. The swept sine started at 1 Hz and ended at 3 Hz and the frequency increasing rate was constant. The whole sweep sine period for each system was lasted 180 s. Base excitation amplitude was 6 mm and the external resistor was 7 Ω for both systems. The test results are shown in Fig. 10. It can be observed that the

Table 3
System parameters.

Symbol	Quantity	Definition
m	31.8 kg (70 lbs.)	Payload mass
m_e	20.9 kg	Equivalent inerter from generator, small generator inertia (1.2×10^{-6}kg·m^2) amplified by 1:33 gearhead (see Eq. (4))
k	6300 N/m	Spring stiffness
R_{ex}	7 Ω	External resistance
c_m	85 Ns/m	Mechanical damping
n	33	Gear ratio
r	7.9×10^{-3} m	Radius of pinion gear
R_i	0.4 Ω	Internal resistance in generator
k_e	1200 rpm/V	Speed constant of generator
k_t	8.0×10^{-3} Nm/A	Torque constant of generator

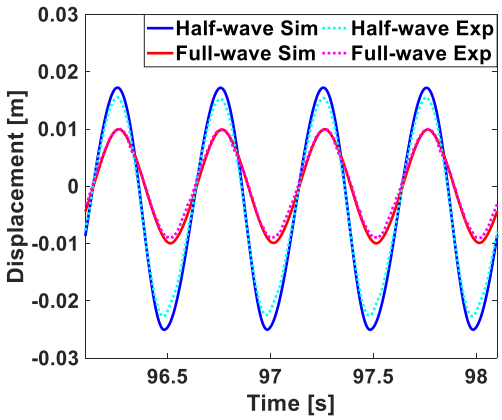

Fig. 8. Time history of displacement under 2 Hz/6 mm base-excitation with a 31.8 kg payload mass.

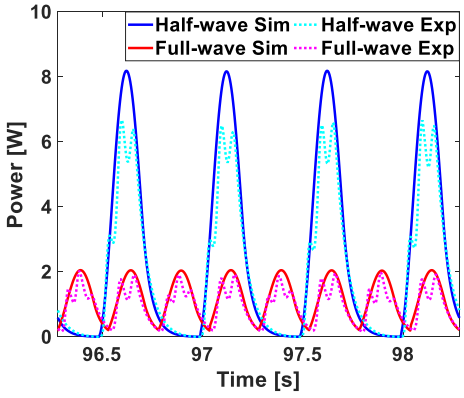

Fig. 9. Time history of output power under 2 Hz/6 mm base-excitation with a 31.8 kg payload mass.

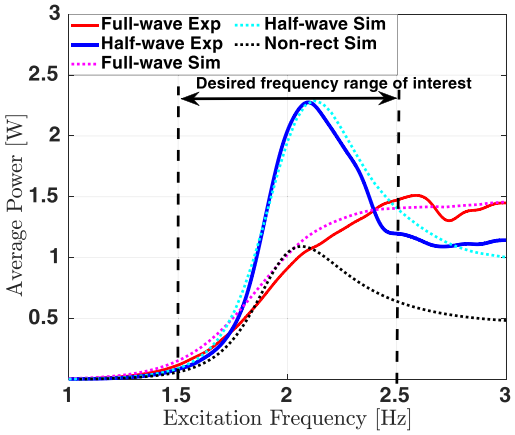

Fig. 10. Frequency responses of output power for both full-wave and half-wave mechanical motion rectification in comparison with the traditional non-rectification under 6 mm swept-sine (1–3 Hz) base excitation.

half-wave mechanical rectification system can achieve about 2 times average of average output power than both full-wave mechanical rectification system and traditional non-rectification system at primary frequency while maintaining larger output power in the desired frequency range. It can be observed from Fig. 10 that the full-wave mechanical rectification system can obtain same output power as the traditional non-rectification system at primary excitation frequency while maintaining larger output power in the desired frequency range,

the same as shown in reference [28]. However, it can be observed that the half-wave mechanical rectification system can not only achieve about twofold average output power as both the full-wave mechanical rectification system and traditional non-rectification system at primary frequency, but can also maintain larger output power in the desired frequency range.

4.2. Treadmill tests

To evaluate the performance and characteristic under real walking, two males participated in the treadmill test. The height of Subject A (25 years old) is 1.7 m and the body weight is 58 kg. The height of Subject B (29 years old) is 1.8 m and the body weight is 80 kg. Considering the participants' load-bearing capacity, the primary payload mass used in the treadmill tests was 13.6 kg and the primary walking speed was desired as 4.8 km/h (i.e. 3 mph). A U.S. Army Military Marine pack system (USMC FILBE Gen II Coyote) was used to assemble the suspended energy harvesting backpack, as shown in Fig. 11. The original plastic stiffener in the military pack system was removed and replaced with a metal frame. The harvester was mounted on the frame and the lower end of the rack was connected to the payload via a force sensor. It should be noted that the harvester used in treadmill tests is the same as bench tests. The payload was connected to a moving board and guided by a pair of rail guides. The upper-ends of the springs were connected on the frame and the lower-ends of springs were connected to the payload mass. A laser displacement sensor was mounted on the frame to measure relative displacement between the payload and frame. The length of the strap can be adjusted to fit different wearers. Fig. 12 shows the treadmill test set-up. All the parameters were kept the same as shown in Table 3, excluding spring stiffness, external resistance and payload mass. Numerical methods were used to determine optimal spring stiffness and electrical damping (i.e. external resistance) under 2 Hz/25 mm base excitation with 13.6 kg payload, as shown in Fig. 13. From Fig. 13 we can see that the half-wave mechanical rectification system can achieve about 4.5 W average power while only 2.5 W for the counterparts under the same payload mass and excitation conditions (25 mm/2 Hz). Fig. 13 shows the traditional non-rectification system has the largest optimal spring stiffness (about 5000–6000 N/m), the half-wave mechanical rectification system has the smallest optimal spring stiffness (about 2500–3200 N/m), and the optimal spring stiffness for the full-wave mechanical rectification system is about 2700–3500 N/m. However, since it is hard to get commercialized springs with the exact stiffness needed, the spring stiffness was chosen as 2767 N/m (i.e. 15.8 lbs./in) for the half-wave mechanical rectification system, while 3037 N/m (i.e. 17.34 lbs./in) was chosen for the full-wave mechanical rectification system.

Xu [35] investigated the interactivity between suspended-load backpack and human gait, and the author found that the leg can be modeled as an inverse pendulum and the center of mass movement would be an arc trajectory in the contact period in a gait cycle. By

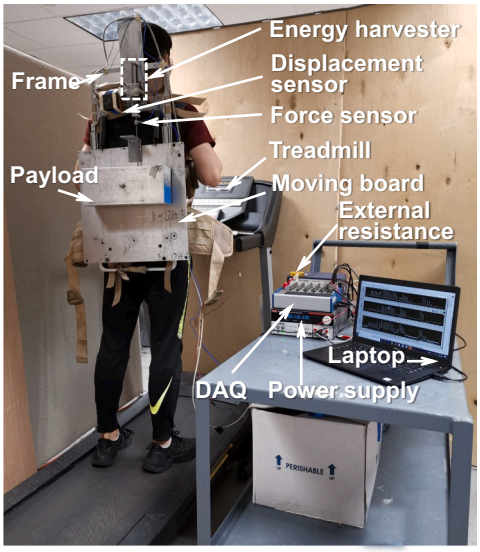

Fig. 12. Treadmill test setup.

modelling as an inverse pendulum, the dominant frequency (ω_b) and amplitude of the torso excitation (Y_b) can be written as a function of leg length (l_0) and walking velocity, as shown in Eq. (11) and Eq. (12). Anthropometry data showed that leg length accounts for 53% of stature [36], therefore the estimated dominant walking frequency and center of mass amplitude for the two test subjects A and B under different walking speed is shown in Fig. 14. It should be noted that the aforementioned inverse pendulum is a pure simple theoretical model. Human walking gait is very complicated and will be affected by gender, age, physical constitution and load mass. The human walking gait model was used to estimate performance and was compared with experiment results.

$$\omega_b = 2\pi^*1.504\left(\frac{V_b}{l_0}\right)^{0.57}\ (s^{-1}) \tag{11}$$

$$Y_b = 0.5l_0\left(1-\sqrt{1-\left(\frac{0.963V_b}{l_0{}^*2^*1.504\left(\frac{V_b}{l_0}\right)^{0.57}}\right)^2}\right) - 0.0157l_0 \tag{12}$$

Both human subjects A and B were orally briefed on the purpose, risks, and benefits of the study at the beginning of the experiment period. Before the scheduling of the real test, the two subjects became familiarized with the suspended backpack, the different walking speeds on the treadmill, and the payload levels. During the real test session, each subject wore the backpack system and adjusted the strap length to make sure the backpack system fit well with the body. Then, the subject

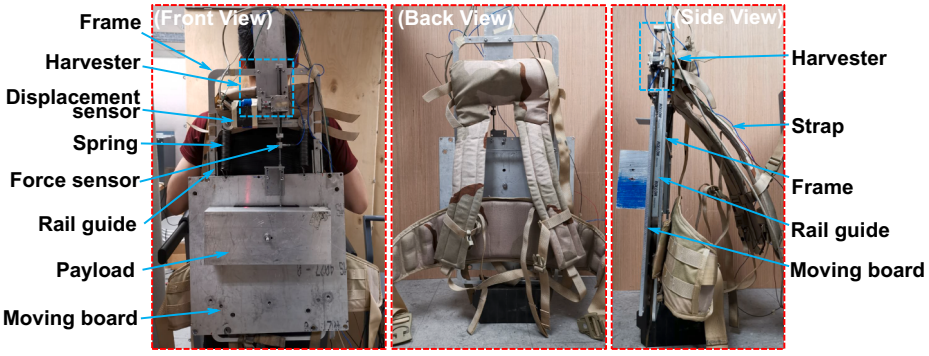

Fig. 11. Prototype assembly for treadmill test.

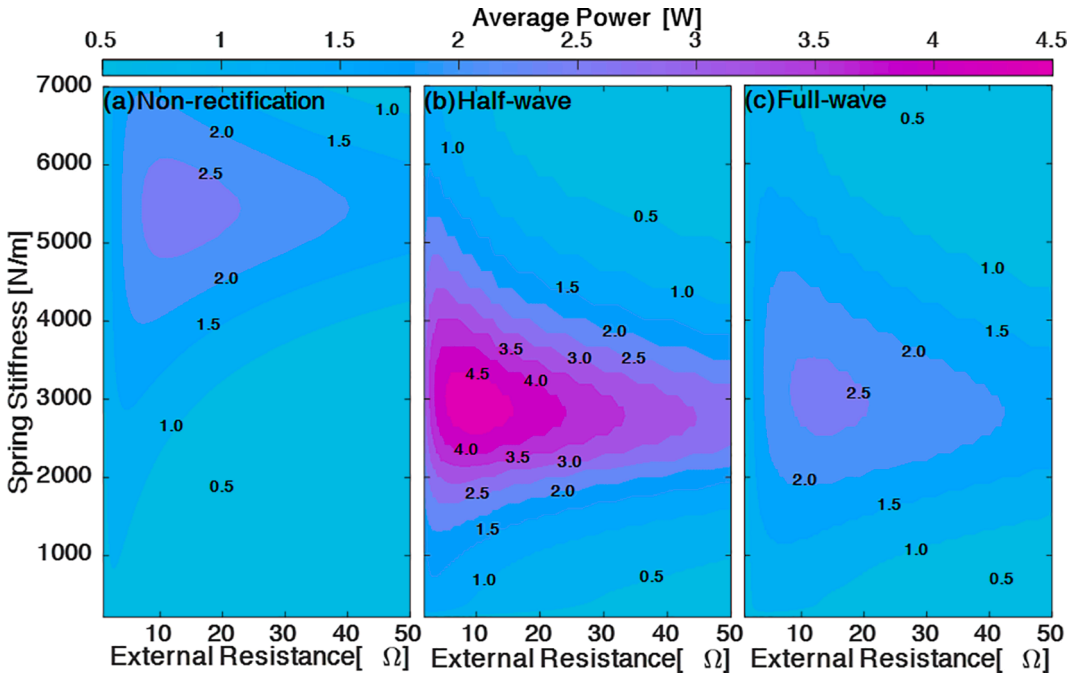

Fig. 13. Average power versus spring stiffness and external resistance under 2 Hz/25 mm base excitation with a 13.6 kg payload.

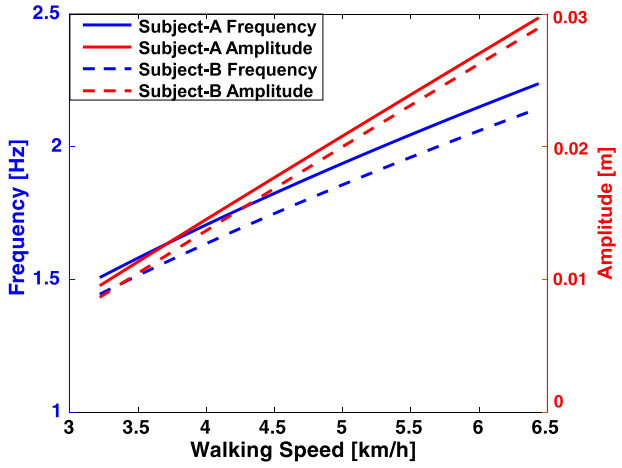

Fig. 14. Estimated dominant walking frequency and center of mass amplitude under different walking speed.

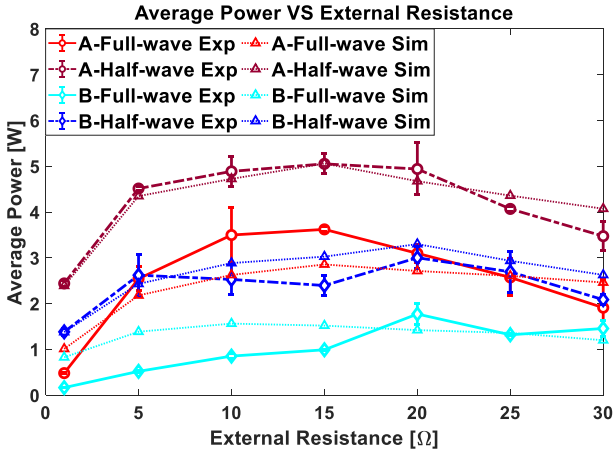

Fig. 15. Average power versus external resistance under different walking speeds with a 13.6 kg backpack payload at desired walking speed 4.8 km/h for two human subjects A and B.

was given 5–10 min to warm up and prepare the legs and torso muscles. For each test trial, the subject set the treadmill at a start speed of 1.6 km/h (i.e. 1 mph) and then increased to the desired speed gradually. The treadmill speed was controlled by the subject. Once the desired speed was reached, the subject walked at the constant speed for 90 s, and only the last 60 s was recorded and analyzed. Then, the subject sat down and rested 2 min before the next test. Each test condition was repeated three times and the subject rested 5 min before the next experiment condition. During the 5 min of rest period, the subject took off the suspended backpack system and the experiment assistant tuned the system, such as external resistance and payload mass, to make sure the prototype was ready for the next desired test condition. Considering the participant's physical condition, each subject only took about 1-hour test in a single day.

Since the desired primary working condition was a 13.6 kg payload under a 4.8 km/h (i.e. 3 mph) walking speed, the first step was to figure out optimal electrical damping (i.e. external resistance), as shown in Fig. 15. It shows the optimal external resistance for subject A is around 15 Ω, while 20 Ω for subject-B, which generally matches the numerical value reported in Fig. 13. In addition, for both subjects, the half-wave mechanical rectification system can achieve higher average power than the full-wave counterpart under the same walking conditions. Fig. 16 shows the average power and specific power (watts per kg) under different walking speeds with the primary payload (13.6 kg) and optimal external resistance (tuned for primary walking speed 4.8 km/h). It should be noted that, Fig. 10 shows the performance will suffer if the excitation frequency is off from the primary frequency. However, Fig. 16 shows that higher walking speeds (i.e. higher frequency) can achieve higher output power. The reason is Fig. 10 is based on a constant excitation amplitude while the center of mass amplitude will increase in high walking speed. Another thing that should be noted from Fig. 16 is that the performances under high walking speed (4.8 km/h) are much less than the theoretical estimation. The reason is the displacement under high walking speed will reach the stroke limit (16 cm) of the rack-pinion set. Fig. 17 shows the average power and specific power under

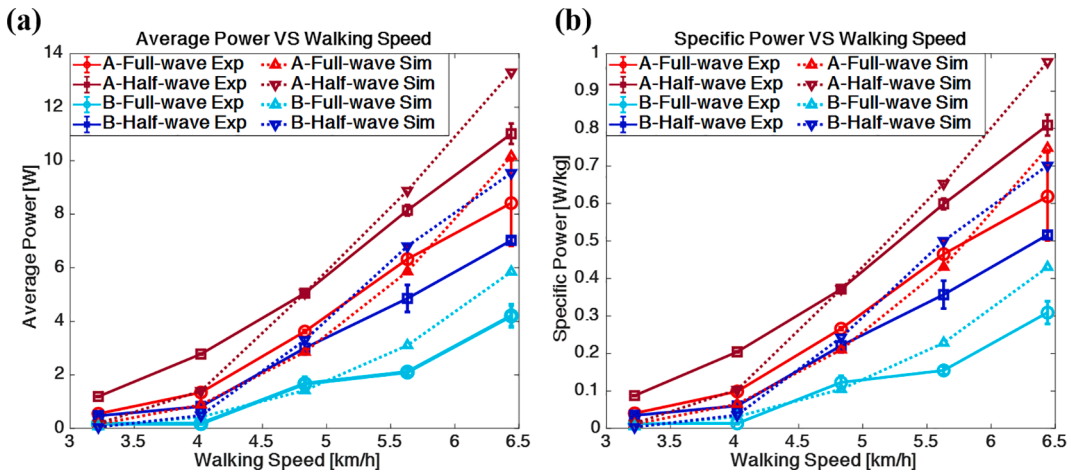

Fig. 16. Performance under different walking speeds with primary backpack payload (13.6 kg) and optimal external resistance and spring stiffness (tuned for primary load mass and primary walking speed) for two human subjects A and B: (a) Average Power (b) Specific Power.

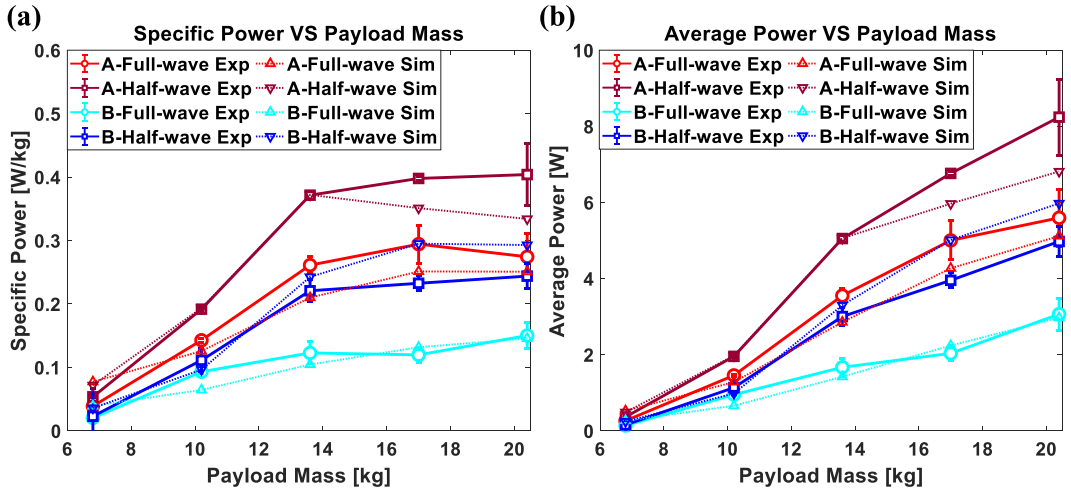

Fig.17. Performance under different backpack payload masses at primary walking speed (4.8 km/h) and optimal external resistance and spring stiffness (tuned for primary load mass and primary walking speed) for two human subjects A and B: (a) Average Power (b) Specific Power.

different payload mass with primary walking speed (4.8 km/h) and optimal external resistance and spring stiffness (for primary walking speed 4.8 km/h). From Fig. 17 we can see the average power will increase with increase of payload mass. However, the specific power will stay in a certain range if the payload mass is larger than the primary mass (13.6 kg). That means the specific power is much more dependent on walking speed (i.e. dominant excitation frequency).

Fig. 18 shows the time history of displacement, force from harvester and output power. Fig. 18(a) shows the time-domain instant results for Subject A under a 4.0 km/h walking speed with a 13.6 kg payload and 15 Ω external resistance. Fig. 18(b) shows the time-domain instant results for Subject B under a 4.8 km/h walking speed with a 13.6 kg payload and 10 Ω external resistance. Fig. 18(a) shows the average power of half-wave mechanical rectification is about 1.8 times higher than the full-wave mechanical rectification system (2.8 W for half-wave mechanical rectification system v.s. 1.6 W for full-wave mechanical rectification system), and Fig. 18(b) shows the average power of half-wave mechanical rectification is about 3.0 times higher than the full-wave mechanical rectification system (2.7 W for half-wave mechanical rectification system v.s. 0.9 W for full-wave mechanical rectification system). Fig. 18 shows the displacement in the half-wave mechanical rectification system is asymmetrical in upward (smaller) and downward (larger) motions, while it obtains symmetrical displacement for the full-wave system. The reason is the generator is engaged only in one vibration direction in the half-wave mechanical rectification system. Therefore, the force from harvester will only appear when the payload moves upwards relatively (and human center of mass moves downwards) in the half-wave mechanical rectification system, while it appears to be a bidirectional symmetrical harvester force for the full-wave mechanical rectification system. Fig. 18 also indicates the half-wave mechanical rectification system acquired 100% larger displacement and 20% more peak force than the full-wave mechanical rectification system. This might be one potential shortcoming for some vibration energy harvesting applications where the vibration stroke is limited by the physical space constraint or the peak force is a concern for human comfort [29]. In the future, methods to decrease the payload stroke or peak force in the half-way mechanical motion rectification shall be investigated. In addition, self-tuning and charging electrical circuit to enable active control [37], and energy management [38], are also potential research topics.

5. Conclusions

In this paper, a vibration energy harvester using novel half-wave mechanical rectification for the application of suspended energy harvesting backpack has been investigated and compared with traditional

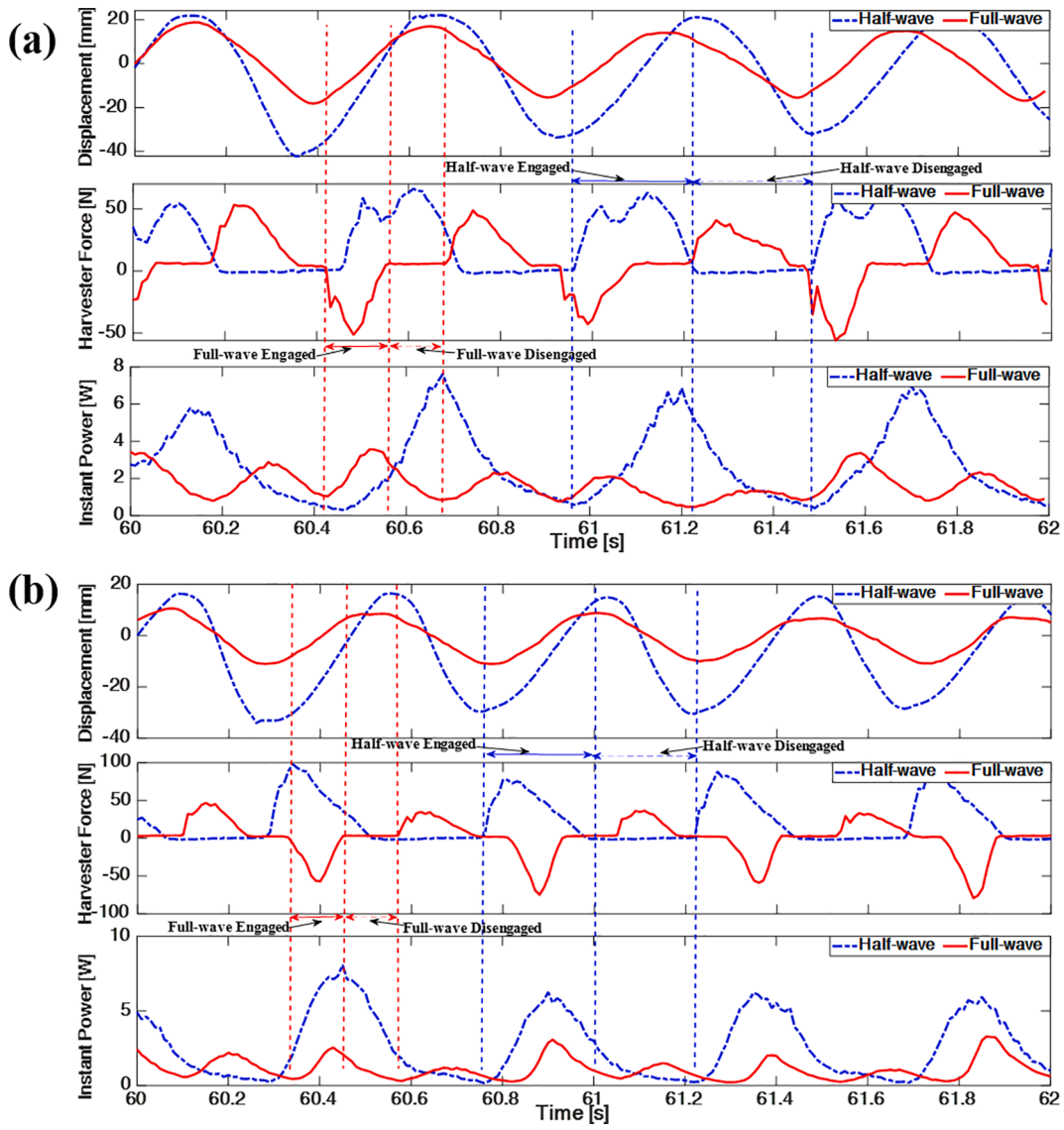

Fig. 18. Time history of treadmill test results. (a) Subject A with 13.6 kg payload under 4.0 km/h(b) Subject B with 13.6 kg payload under4.8 km/h.

non-rectification and full-wave mechanical rectification mechanisms. Bench tests and treadmill tests have been conducted to investigate the performance. The results indicate that the proposed suspended energy harvesting backpack could continuously generate an amount of electricity suitable for powering portable and wearable electronic devices which can may be applied to the military, field workers, outdoor enthusiasts and disaster relief scenarios. The conclusions drawn from the investigation are as follows:

1. The proposed half-wave mechanical rectification mechanism can convert bidirectional linear motion into unidirectional rotation with nonlinear inertia.
2. Dynamic modeling and numerical simulation show the proposed half-wave mechanical rectification-based energy harvesting backpack can obtain about twofold average output power as the previous full-wave mechanical rectification-based design while maintaining larger output power in the target broad frequency range at the same time.
3. Bench test results indicate the proposed half-wave mechanical rectification-based energy harvesting backpack can harvest 6.7 W (peak)/2.1 W (average) under 2 Hz/6 mm base-excitation with a 31.8 kg (70 lbs.) payload, which is a significant improvement compared with 1.9 W(peak)/0.9 W (average) for the counterpart full-wave mechanical rectification-based system.
4. Under a walking speed of 4.8 km/h (3 mph), treadmill tests demonstrate an average power range of 3.3–5.1 W and the specific power can reach 0.4 W/kg with a 13.6 kg (30 lbs.) payload.
5. Treadmill tests indicates the proposed half-wave mechanical rectification system will obtain larger displacement and 20% larger peak force from harvester than the counterpart full-wave mechanical rectification system.

CRediT authorship contribution statement

Jia Mi: Conceptualization, Methodology, Investigation, Validation, Writing - original draft, Visualization. **Qiaofeng Li:** Software, Formal analysis, Investigation, Writing - review & editing. **Mingyi Liu:** Conceptualization, Methodology, Investigation, Writing - review & editing. **Xiaofan Li:** Data curation, Formal analysis. **Lei Zuo:** Supervision, Project administration, Funding acquisition, Writing - review & editing.

Declaration of Competing Interest

The authors declare that they have no known competing financial interests or personal relationships that could have appeared to influence the work reported in this paper.

Acknowledgement

The authors would like to thank the partial funding support from the U.S. National Science Foundation (NSF) through Award 1903627 and the U.S. Office of Naval Research (ONR) through Award N00014-17-1-2225. The authors would like to thank Joseph Capper and Erin Jones for the proof reading.

References

[1] Kuo AD. Harvesting energy by improving the economy of human walking. Science 2005;309(5741):1686–7.
[2] Tholl MV, Akarçay HG, Tanner H, Niederhauser T, Zurbuchen A, Frenz M, et al. Subdermal solar energy harvesting – a new way to power autonomous electric implants. Appl Energy 2020;269:114948.
[3] Yuan Y, Liu M, Tai WC, Zuo L. Design and treadmill test of a broadband energy harvesting backpack with a mechanical motion rectifier. J Mech Des 2018;140(8).
[4] Wang W, Cao J, Zhang N, Lin J, Liao WH. Magnetic-spring based energy harvesting from human motions: design, modeling and experiments. Energy Convers Manage 2017;132:189–97.
[5] Akhtar F, Rehmani MH. Energy replenishment using renewable and traditional energy resources for sustainable wireless sensor networks: a review. Renew Sustain Energy Rev 2015;45:769–84.
[6] Prauzek M, Konecny J, Borova M, Janosova K, Hlavica J, Musilek P. Energy harvesting sources, storage devices and system topologies for environmental wireless sensor networks: a review. Sensors 2018;18(8):2446.
[7] McArdle WD, Katch FI, Katch VL. Exercise physiology: energy, nutrition, and human performance; 1991.
[8] Guo H, Pu X, Chen J, Meng Y, Yeh MH, Liu G, et al. A highly sensitive, self-powered triboelectric auditory sensor for social robotics and hearing aids. Sci Robot 2018;3(20):eaat2516.
[9] Yang R, Qin Y, Li C, Zhu G, Wang ZL. Converting biomechanical energy into electricity by a muscle-movement-driven nanogenerator. Nano Lett 2009;9(3):1201–5.
[10] Dong L, Han X, Xu Z, Closson AB, Liu Y, Wen C, et al. Flexible porous piezoelectric cantilever on a pacemaker lead for compact energy harvesting. Adv Mater Technol 2019;4(1):1800148.
[11] Qian F, Xu TB, Zuo L. Piezoelectric energy harvesting from human walking using a two-stage amplification mechanism. Energy 2019;189:116140.
[12] Kuang Y, Ruan T, Chew ZJ, Zhu M. Energy harvesting during human walking to power a wireless sensor node. Sens Actuators A: Phys 2017;254:69–77.
[13] Yuan J, Zhu R. A fully self-powered wearable monitoring system with systematically optimized flexible thermoelectric generator. Appl Energy 2020;271:115250.
[14] Riemer R, Shapiro A. Biomechanical energy harvesting from human motion: theory, state of the art, design guidelines, and future directions. J NeuroEng Rehabil 2011;8(1):22.
[15] Donelan JM, Li Q, Naing V, Hoffer JA, Weber DJ, Kuo AD. Biomechanical energy harvesting: generating electricity during walking with minimal user effort. Science 2008;319(5864):807–10.
[16] Rome LC, Flynn L, Goldman EM, Yoo TD. Generating electricity while walking with loads. Science 2005;309(5741):1725–8.
[17] Douglas JS. Preliminary analysis of energy harvesting assault pack. US army CERDEC CP&ID power division; 2015. https://ndiastorage.blob.core.usgovcloudapi.net/ndia/2015/power/17829douglas.pdf [accessed Apr 15th 2020].
[18] Matsumoto Y, Nishioka T, Shiojiri H, Matsuzaki K. Dynamic design of footbridges. IABSE-Proc. P-17/78, S. 1–15. IABSE-AIPC-IVBH, Zürich; 1978.
[19] Bachmann H, Ammann WJ, Deischl F, Eisenmann J, Floegl I, Hirsch GH, et al. Vibration problems in structures: practical guidelines. Birkhäuser 2012.
[20] Abdelkareem MA, Xu L, Ali MKA, Elagouz A, Mi J, Guo S, et al. Vibration energy harvesting in automotive suspension system: a detailed review. Appl Energy 2018;229:672–99.
[21] Guo, S., Chen, Z., Guo, X., Zhou, Q., & Zhang, J. (2014). *Vehicle interconnected suspension system based on hydraulic electromagnetic energy harvest: design, modeling and simulation tests* (No. 2014-01-2299). SAE Technical Paper.
[22] Zhu D, Tudor MJ, Beeby SP. Strategies for increasing the operating frequency range of vibration energy harvesters: a review. Measur Sci Technol 2009;21(2):022001.
[23] Tai WC, Zuo L. On optimization of energy harvesting from base-excited vibration. J Sound Vibrat 2017;411:47–59.
[24] Wang W, Cao J, Bowen CR, Zhou S, Lin J. Optimum resistance analysis and experimental verification of nonlinear piezoelectric energy harvesting from human motions. Energy 2017;118:221–30.
[25] Gupta A, Jendrzejczyk JA, Mulcahy TM, Hull JR. Design of electromagnetic shock absorbers. Int J Mech Mater Des 2006;3(3):285–91.
[26] Li Z, Zuo L, Kuang J, Luhrs G. Energy-harvesting shock absorber with a mechanical motion rectifier. Smart Mater Struct 2012;22(2):025008.
[27] Zou HX, Zhao LC, Gao QH, Zuo L, Liu FR, Tan T, et al. Mechanical modulations for enhancing energy harvesting: Principles, methods and applications. Appl Energy 2019;255:113871.
[28] Liu M, Tai WC, Zuo L. Toward broadband vibration energy harvesting via mechanical motion-rectification induced inertia nonlinearity. Smart Mater Struct 2018;27(7):075022.
[29] Liu M, Tai WC, Zuo L. Enhancing the performance of backpack energy harvester using nonlinear inerter-based two degrees of freedom design. Smart Mater Struct 2020;29(2):025007.
[30] Mi J, Xu L, Zhu Z, Liu M, Zuo L. Design, modeling and testing of a one-way energy harvesting backpack. In: Active and passive smart structures and integrated systems XII, vol. 10595. International Society for Optics and Photonics; 2018, April. p. 1059520.
[31] Zhu Z, Xu L, Abdelkareem MA, Zou J, Mi J. Design and simulation analysis of vibration energy harvesting system based on ADAMS. In: International design engineering technical conferences and computers and information in engineering conference, vol. 59285. American Society of Mechanical Engineers; 2019. p. V008T10A011.
[32] Pan Y, Lin T, Qian F, Liu C, Yu J, Zuo J, et al. Modeling and field-test of a compact electromagnetic energy harvester for railroad transportation. Appl Energy 2019;247:309–21.
[33] Liu M, Lin R, Zhou S, Yu Y, Ishida A, McGrath M, et al. Design, simulation and experiment of a novel high efficiency energy harvesting paver. Appl Energy 2018;212:966–75.
[34] Smith MC. Synthesis of mechanical networks: the inerter. IEEE Trans Automatic Control 2002;47(10):1648–62.
[35] Xu X. An Investigation on the Interactivity between Suspended-load Backpack and Human Gait; 2008.
[36] Roebuck JA, Kroemer KH, Thomson WG. Engineering anthropometry methods, vol. 3. John Wiley & Sons, 1975.
[37] Liu M, Zuo L, Jung H, Sharma Y. Electrical damping tuning for broad bandwidth and human comfortable in backpack energy harvesting (Conference Presentation). In: Smart structures and NDE for industry 4.0, smart cities, and energy systems, vol. 11382. International Society for Optics and Photonics; 2020. p. 113820A.
[38] Zhou Q, Li J, Shuai B, Williams H, He Y, Li Z, et al. Multi-step reinforcement learning for model-free predictive energy management of an electrified off-highway vehicle. Appl Energy 2019;255:113755.